REPORT DOCUMENTATION PAGE

AFRL-SR-BL-TR-01-

0070

1. AGENCY USE ONLY *(Leave blank)*	2. REPORT DATE	3. REPORT TYPE AND DATES COVERED
		15 Mar 97 to 14 Mar 98 Final

4. TITLE AND SUBTITLE
(DURIP-97) Advanced Optoelectronic systems Using Fiber Amplifiers and Lasers

5. FUNDING NUMBERS
61103D
3484/US

6. AUTHOR(S)
Dr. Fetterman

7. PERFORMING ORGANIZATION NAME(S) AND ADDRESS(ES)
University of California, Los Angeles
1400 Uberroth Bldg. Box 951406
Los Angeles, CA 90095-1406

8. PERFORMING ORGANIZATION REPORT NUMBER

9. SPONSORING/MONITORING AGENCY NAME(S) AND ADDRESS(ES)
AFOSR/NE
801 North Randolph Street, Rm 732
Arlington, VA 22203-1977

10. SPONSORING/MONITORING AGENCY REPORT NUMBER
F49620-97-1-0189

11. SUPPLEMENTARY NOTES

12a. DISTRIBUTION AVAILABILITY STATEMENT
Unlimited Distribution

12b. DISTRIBUTION CODE

13. ABSTRACT *(Maximum 200 words)*

The DURIP equipment permitted us to do a number of unique studies at 1.5 microns for the first time. Until this point we were largely confined to 1.3 microns which had limited application to communications and new optical systems. In particular, using a wavelength slicing technique, with this equipment, we have studied optical delays and group velocity dispersion in novel fiber gratings made by Professor Feinberg of USC.

14. SUBJECT TERMS			15. NUMBER OF PAGES
			16. PRICE CODE
17. SECURITY CLASSIFICATION OF REPORT	18. SECURITY CLASSIFICATION OF THIS PAGE	19. SECURITY CLASSIFICATION OF ABSTRACT	20. LIMITATION OF ABSTRACT
UNCLASSIFIED	UNCLASSIFIED	UNCLASSIFIED	UL

UNIVERSITY OF CALIFORNIA, LOS ANGELES

BERKELEY • DAVIS • IRVINE • LOS ANGELES • RIVERSIDE • SAN DIEGO • SAN FRANCISCO

SANTA BARBARA • SANTA CRUZ

ELECTRICAL ENGINEERING DEPARTMENT
THE HENRY SAMUELI SCHOOL OF ENGINEERING
AND APPLIED SCIENCE
BOX 951594
LOS ANGELES, CALIFORNIA 90095-1594

Jan. 2, 2001

Dr. Howard Schlossberg
Air Force Office of Scientific Research
801 North Randolph Street, Room 732
Arlington VA 22203-1977

Dear Dr. Schlossberg:

I enclose the Final Technical report for the DURIP grant # F49620-97-1-0189. The equipment bought under this grant was absolutely vital in getting a number of major new efforts going. In particular the mode locked, ultrashort pulse laser, in combination with the erbium amplifier and optical spectrum analyzer permitted us to examine fiber gratings, optical A to D systems and phased array radars in extremely novel configurations.

This equipment continues to be the very heart of several new efforts in our high frequency optical interactions program. I thank you again for your support in this effort.

Sincerely yours,

Harold Fetterman

Advanced Optoelectronic System Development

DURIP
F49620-97-1-0189

Harold Fetterman, UCLA

The DURIP equipment permitted us to do a number of unique studies at 1.5 microns for the first time. Until this point we were largely confined to 1.3 microns which had limited application to communications and new optical systems.

In particular, using a wavelength slicing technique, with this equipment, we have studied optical delays and group velocity dispersion in novel fiber gratings made by Professor Feinberg of USC.

Another set of measurements used the extraordinary bandwidth of these lasers to effectively time stretch analogy signals and transform them to lower frequencies. This was demonstrated up to 100 GHz.

Finally, the optical spectrum analyzer also permitted us to implement our new optical controlled phased array technology using a serial feed with fast tunable lasers.

For each case we have included examples of papers that we have published using the equipment bought under this program. In addition to the work currently in progress using this equipment, at least four other researchers have also used this equipment for specific measurements which could not otherwise be done at the University.

Thank you very much again for support of this effort.

MEASUREMENT OF THE TEMPORAL DELAY OF A LIGHT PULSE THROUGH A ONE-DIMENSIONAL PHOTONIC CRYSTAL

Shamino Wang,[1] Hernan Erlig,[1] Harold R. Fetterman,[1] Eli Yablonovitch,[1] Victor Grubsky,[2] Dmitry S. Starodubov,[2] and Jack Feinberg[2]
[1] Department of Electrical Engineering
University of California
Los Angeles, California 90095
[2] Department of Physics
University of Southern California
Los Angeles, California 90089-0484

Received 4 June 1998

ABSTRACT: *We measure a maximum group delay of 22.6 ps for a light pulse propagating through a 1 cm long fiber Bragg grating when the frequency of the light is tuned near the band edge of the grating. Our measurements are performed in the time domain with single picosecond resolution using wavelength-tunable pulses of 0.5 nm bandwidth spectrally sliced from a mode-locked laser. Our experimental results are qualitatively confirmed by our numerical simulations. Promising applications include optical delay elements for phased-array radar and encoders/decoders in spread-spectrum code-division multiple-access systems.* © 1999 John Wiley & Sons, Inc. Microwave Opt Technol Lett 20: 17–21, 1999.

Key words: *group delay; fiber Bragg grating; photonic crystal; wavelength slicing; code-division multiple access*

A one-dimensional photonic crystal is a periodic array of layers with different indexes of refraction. Light propagating at frequencies near the stopband of a photonic crystal will be delayed and dispersed [1], which may prove useful for optically controlled phased-array radars [2]. To date, experimental efforts to measure such delays have been in the frequency domain [3], or in the time domain with a 50 GHz sampling oscilloscope [4]. In this paper, we directly measure the group delay in the time domain with single picosecond resolution, and show that the delay increases as the frequency of the pulse approaches the edge of the photonic crystal's stopband.

We used a Bragg grating in an optical fiber as the one-dimensional photonic crystal. The grating measured ~1 cm in length, had a 1553.20 nm central wavelength, and a 2.10 nm, 3 dB bandwidth. We first theoretically analyzed the physical properties of such a structure using a commercial grating simulation program (IFO_Gratings). To match the actual grating's spectral characteristics, our simulated fiber Bragg grating had a 1 cm long uniform quarter-wave structure and a 0.0035 refractive index change between layers. Figure 1 shows the transmission spectrum and the group velocity as a function of wavelength for the simulated grating. The computed group velocity is seen to drop sharply as the central wavelength of the pulse approaches the edge of the bandgap. Therefore, a tunable delay can be achieved by varying the central wavelength of the propagating pulse with respect to the reflection edge of the grating.

To measure the delay induced by the actual grating, we used the tunable picosecond source shown in Figure 2. The 1.55 μm mode-locked erbium-doped fiber laser emitted a 160 fs (FWHM) pulse train with a 56 nm (FWHM) bandwidth. For the experiments here, we needed a tunable source whose bandwidth was smaller than the width of the grating stopband, which is usually on the order of nanometers. To narrow the frequency spectrum of our pulsed laser, we used an HP 71451B optical spectrum analyzer as a wavelength slicer [5]. By selecting the resolution bandwidth of the spectrum analyzer, we could vary the pulse bandwidth from 0.1 to 10 nm. The pulse center wavelength was tuned by selecting slices of different spectral content. An autocorrelator and a second spectrum analyzer were used to perform diagnostic tests. The results are shown in Figure 3. Note that as the pulse's spectral bandwidth decreased, its temporal length increased, as required by the uncertainty principle.

Light from the wavelength-tunable picosecond source was split into two beams. One beam was sent into the fiber containing a Bragg grating, and the other beam was sent into a reference fiber. The two transmitted signals were recombined and sent to an autocorrelator with a scan window ~120 ps. The autocorrelator displayed both the autocorrelation and the cross-correlation traces. The length of the grating arm was made intentionally longer (by ~1 cm) to separate the autocorrelation and cross-correlation traces (by ~56 ps). Any group delay caused by the fiber Bragg grating produced an additional displacement of the cross-correlation trace relative to the autocorrelation trace. The cross-correlation trace also revealed any dispersion caused by propagation through the grating. Note that any dispersion caused by the fiber itself was common to both pulses.

A typical transmission spectrum of the fiber Bragg grating is shown in Figure 4(a). The spectrum analyzer bandwidth was set to chop 0.5 nm wide wavelength slices; the resulting pulses had a ~16 ps (FWHM) autocorrelation. The chopped slices were not Gaussian, and fitted approximately the sinc-squared function predicted from a "top hat" spectral distribution over the range considered here. Correlation traces were obtained as the pulse's central wavelength was positioned at various wavelengths near the grating bandgap. For trace *A* in Figure 4(b), we expected and saw no additional delay from the grating. However, the measured group delays for points *B*, *C*, and *D* increased from the 56 ps value by 1.9, 11.4, and 22.6 ps, respectively, as the central wavelength of the pulse approached the edge of the grating's stopband.

From our simulation, we expected the following trends as the laser wavelength neared the grating bandgap: 1) increasing group velocity delay, 2) increasing dispersion, and 3) reduced transmission due to increased reflectivity nearer the grating. Indeed, traces *B*, *C*, and *D* confirm that: 1) the cross-correlation peaks moved further away from the autocorrelation traces, 2) the cross-correlation traces spread out in time due to increased dispersion, and 3) the peak intensities of the cross-correlation traces dropped because of lower transmission as the bandgap was approached. Similar trends were also observed as the bandgap was approached from

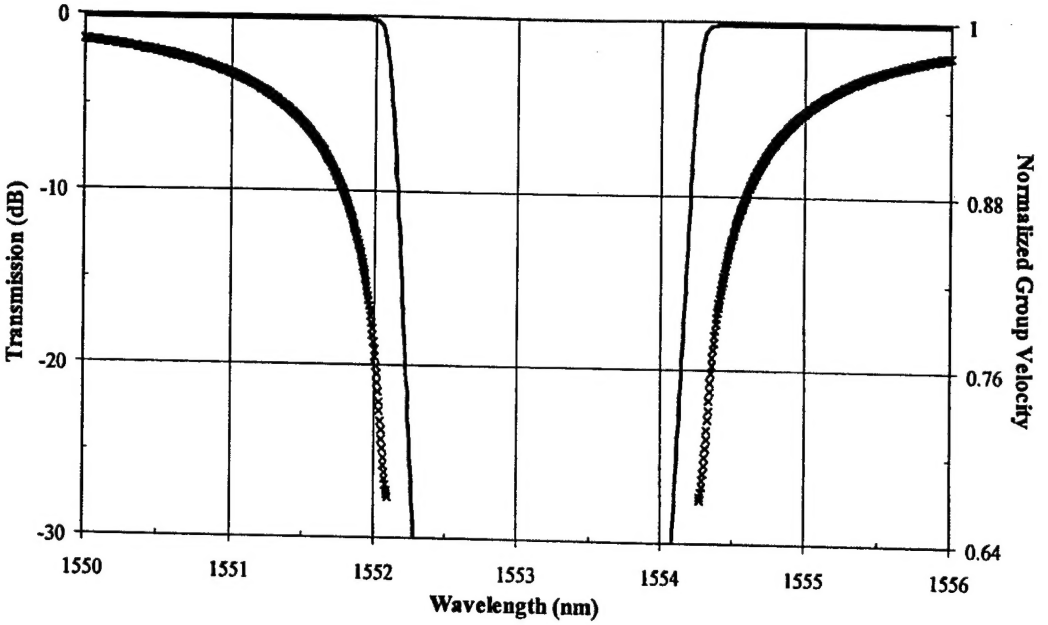

Figure 1 Simulation of a fiber Bragg grating centered at 1553.20 nm with a rectangular index profile. The solid line represents the transmission spectrum and the crosses the group velocities. A refractive index difference between layers of $\Delta = 0.0035$ was used to match the measured spectrum. The group velocities are normalized to the speed of light in bare fiber

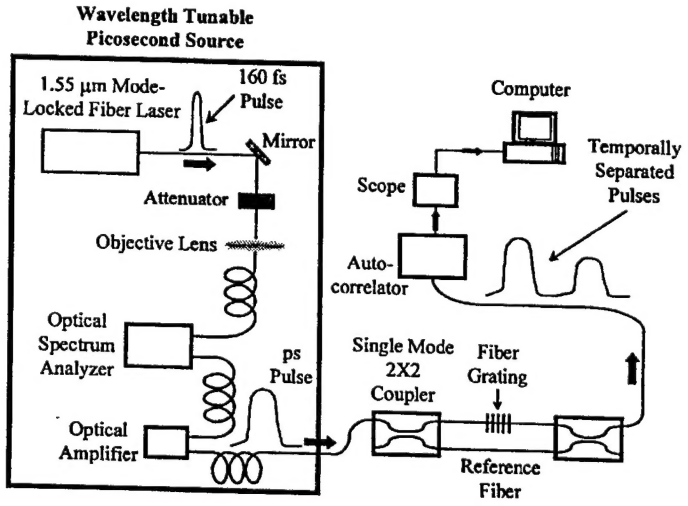

Figure 2 Group delay measurement setup. The autocorrelator displays both the autocorrelation and cross-correlation traces, with the separation between the traces equal to the temporal separation between the reference pulse and the lagging grating pulse

longer wavelengths, as shown in Figure 4. The measured additional group delays for points E and F were 8.2 and 3.1 ps, respectively.

Here, we have clearly demonstrated directly in the time domain that a photonic band structure can serve as a delay line in transmission. The 22.6 ps group delay caused by the grating used here corresponded to a 50% increase in the grating's effective length. That is, the 1 cm Bragg grating was equivalent to a 1.5 cm long delay line. We expect longer delays as the grating parameters are optimized in future experiments. One application for such delay lines is in phased-array radar systems, where the conventional chirped gratings and circulators/couplers might be replaced by simple uniform Bragg gratings.

It has also been proposed that photonic bandgap materials could be used as dispersion compensators[3, 6, 7]. By differentiating the group velocity with respect to wavelength, we find negative group velocity dispersion on the short-wavelength side of the grating bandgap and positive group velocity on the long-wavelength side. In principle, we can design a grating pair with different stopband locations such that positive dispersion from the first grating would compensate negative dispersion from the second grating[8]. In addition, one could put a grating in a transmitter and a second conjugate

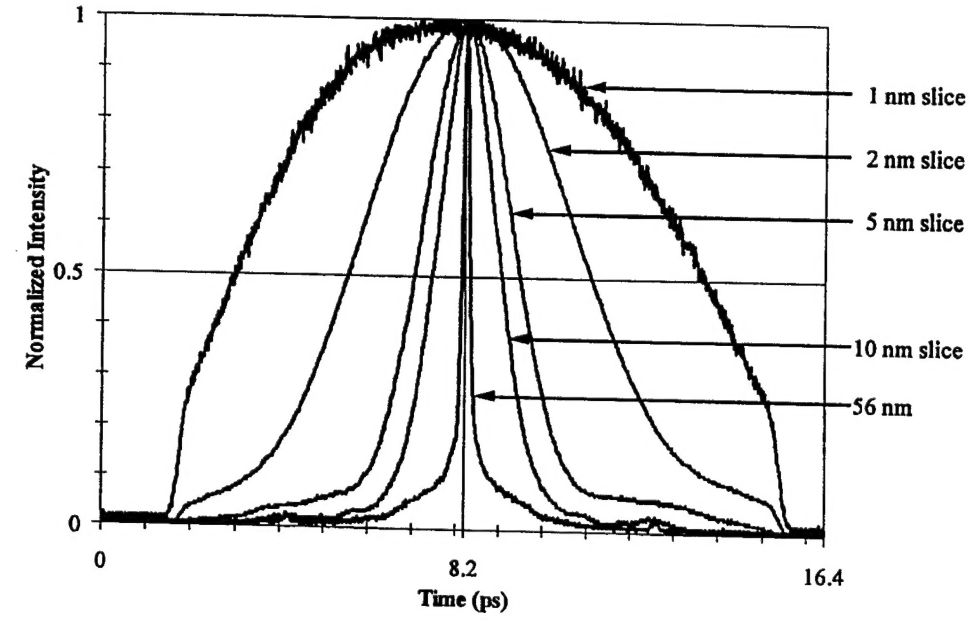

(a)

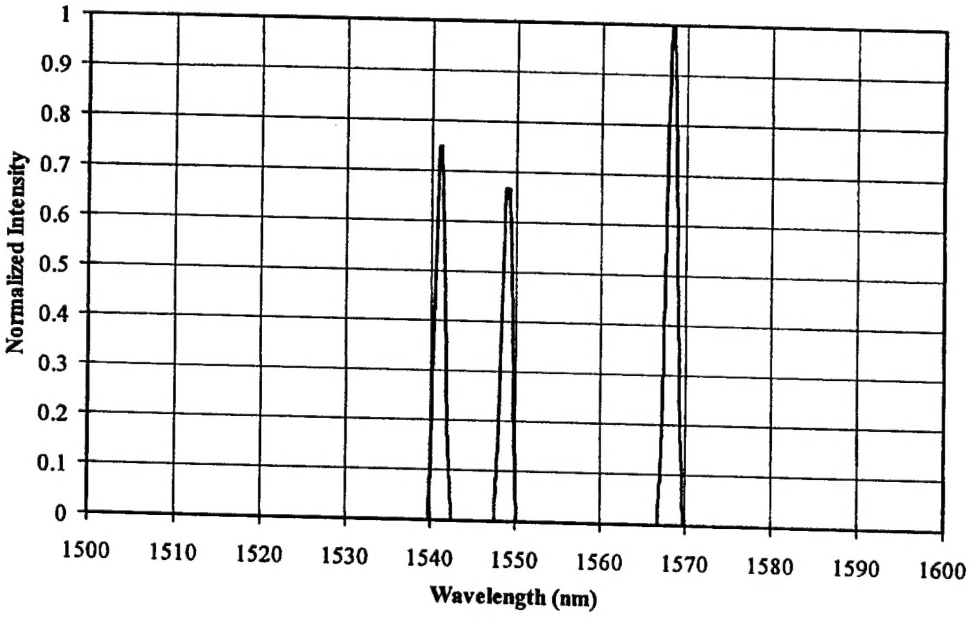

(b)

Figure 3 (a) Autocorrelation traces of the 56 nm(FWHM) bandwidth laser pulse and of various wavelength slices( )b Tunability of a fixed bandwidth slice within the available 56 nm(FWHM) laser bandwidth

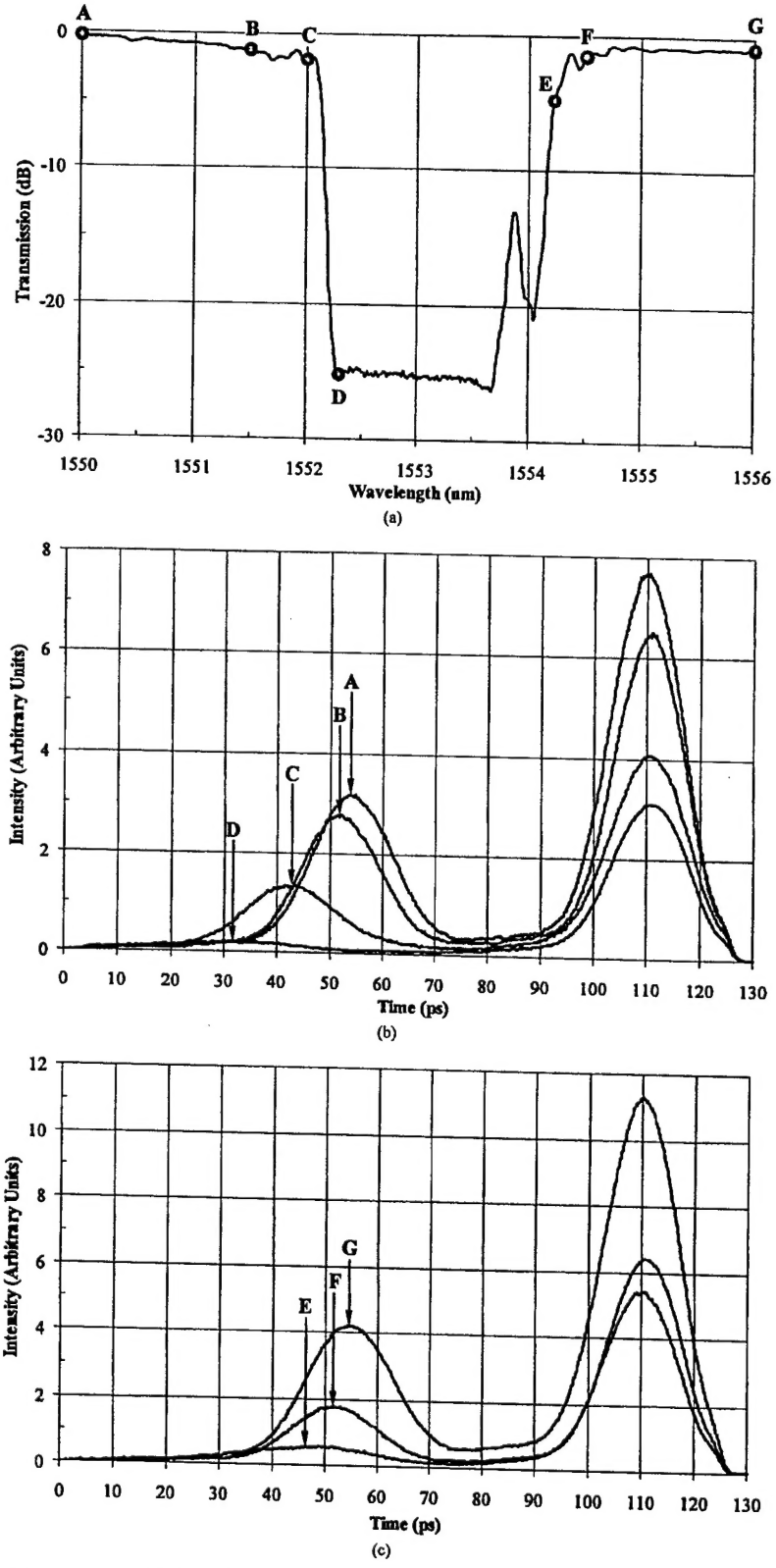

Figure 4 (a) Transmission spectrum of the fiber Bragg grating under test. Operating wavelengths for the points of interest are: 1550.00 nm, *B*: 1551.50 nm, *C*: 1552.00 nm, *D*: 1552.25 nm, *E*: 1554.20 nm, *F*: 1554.50 nm, and *G*: 1556.00 nm. (b) Correlation traces for points *A*, *B*, *C*, and *D*. The autocorrelation traces are located at 110 ps.( ) Correlation traces for points *E*, *F*, and *G*. The autocorrelation traces are located at 110 ps

grating in a receiver for use as encoding/decoding components for spread-spectrum code-division multiple-access matched filter systems.

In conclusion, for the first time, to our knowledge, we have measured in the time domain, with single picosecond resolution, the group velocity delay caused by a pulse propagating near the edge of the stopband of a one-dimensional photonic crystal. Such delays can have practical applications for phased-array radar and matched filter systems.

ACKNOWLEDGMENT

This research was supported by the Air Force Office of Scientific Research (AFOSR) and by the Ballistic Missile Defense Organization (BMDO).

REFERENCES

1. M. Scalora, R.J. Flynn, S.B. Reinhardt, R.L. Fork, M.J. Bloemer, M.D. Tocci, C.M. Bowden, H.S. Ledbetter, J.M. Bendickson, J.P. Dowling, and R.P. Leavitt, Ultrashort pulse propagation at the photonic band edge: Large tunable group delay with minimal distortion and loss, Phys Rev E 54 (1996), R1078–R1081.
2. W.H. Loh, R.I. Laming, N. Robinson, A. Cavaciuiti, F. Vaninetti, C.J. Anderson, M.N. Zervas, and M.J. Cole, Dispersion compensation over distances in excess of 500 km for 10-Gb/s systems using chirped fiber gratings, IEEE Photon Technol Lett 8 (1996), 944–946.
3. B.J. Eggleton, T. Stephens, P.A. Krug, G. Dhosi, Z. Brodzeli, and F. Ouellette, Dispersion compensation using a fibre grating in transmission, Electron Lett 32 (1996), 1610–1611.
4. B.J. Eggleton, C.M. de Sterke, and R.E. Slusher, Nonlinear pulse propagation in Bragg gratings, J Opt Soc Amer B 14 (1997), 2980–2993.
5. T.M. Goyette, W. Guo, F.C. De Lucia, J.C. Swartz, H.O. Everitt, B.D. Guenther, and E.R. Brown, Femtosecond demodulation source for high-resolution submillimeter spectroscopy, Appl Phys Lett 67 (1995), 3810–3812.
6. N.M. Litchinitser, B.J. Eggleton, and D.B. Patterson, Fiber Bragg gratings for dispersion compensation in transmission: Theoretical model and design criteria for nearly ideal pulse recompression, J Lightwave Technol 15 (1997), 1303–1313.
7. N.M. Litchinitser and D.B. Patterson, Analysis of fiber Bragg gratings for dispersion compensation in reflective and transmissive geometries, J Lightwave Technol 15 (1997), 1323–1328.
8. S. Wang, H. Erlig, H.R. Feterman, E. Yablonovitch, V. Grubsky, D.S. Starodubov, and J. Feinberg, submitted to IEEE Microwave Guided Wave Lett.

CCC 0895-2477/99

Group Velocity Dispersion Cancellation and Additive Group Delays by Cascaded Fiber Bragg Gratings in Transmission

Shamino Wang, *Student Member, IEEE,* Hernan Erlig, *Student Member, IEEE,* Harold R. Fetterman, *Fellow, IEEE,* Eli Yablonovitch, *Fellow, IEEE,* Victor Grubsky, Dmitry S. Starodubov, and Jack Feinberg

Abstract— **We have demonstrated that cascaded fiber Bragg gratings can provide delays of propagating pulses with minimal pulse reshaping. The grating pair used exhibited an overlap transmission region centered at 1551.05 nm, where both gratings contribute to the group delay and the group velocity dispersion (GVD) was canceled. Using wavelength tunable pulses spectrally sliced from a mode-locked fiber laser, the measurement was performed in the time domain with single picosecond resolution. Both gratings were 3 mm long and a maximum group delay of 15 ps was measured for the cascaded sequence. This compound grating configuration can be implemented as encoders and decoders in spread spectrum CDMA systems.**

Index Terms— **CDMA, dispersion compensation, fiber Bragg grating, group delay, wavelength slicing.**

I. Introduction

UNIFORM fiber Bragg gratings, essentially one-dimensional photonic crystals, exhibit low group velocity and large dispersion near their stop bands. Therefore, delays can be achieved in transmission at band edge frequencies of uniform gratings, eliminating the need for circulators or couplers in conventional reflection schemes [1]. These delays are also coupled with dispersion, which severely limits their application to communication systems. In this letter we demonstrate that this dispersion can be effectively compensated for by transmission through opposite sides of grating pair stop bands, while both gratings contribute to the additive delay. Simulations have demonstrated the advantages afforded by gratings in long-haul fiber dispersion compensation [2], [3]. So far experimental investigations in this arena have been performed in the frequency domain [4] or in the time domain using a 50-GHz sampling oscilloscope [5]. Previously we reported single picosecond resolution time-domain measurements of group delay incurred by optical pulses propagating through a uniform grating [6]. We also demonstrated that the group delay was additive for nearly identical cascaded gratings; however, the transmitted pulse was severely distorted [7].

In this letter we explore a fiber Bragg grating pair that provided a 15-ps group delay with compensated GVD in transmission. The gratings were 3 mm long each and spatially separated to avoid any coupling effect. The measured transmission spectrum is shown in Fig. 1. The grating pair exhibited bandgap centers at 1550.25 and 1552.10 nm with 3-dB bandwidths of 1.40 and 1.82 nm, respectively. The overlap transmission region had a 1551.05-nm central wavelength, a 0.5-nm 3-dB bandwidth, and −3-dB peak intensity transmission. A commercial simulation program was used to model the gratings with parameters chosen to match the measured transmission spectrum. The simulated group velocities are shown in Fig. 2. The constant effective group velocity from 1550.99 to 1551.10 nm in the overlap transmission region resulted from GVD and higher order dispersion compensation. This was confirmed experimentally in the time domain by the minimal pulse distortion.

II. Experimental Setup

The output from a 1.55-μm mode-locked erbium-doped fiber laser exhibiting a 56-nm bandwidth was spectrally sliced [8] by an HP optical spectrum analyzer. The resulting 0.5-nm bandwidth pulses produced a ~16-ps full-width at half-maximum (FWHM) auto-correlation. Using a 3-dB coupler the pulse train was divided into the grating pair and into a reference fiber, subsequently recombined, and fed to an auto-correlator. The pulse train timing difference was then measured from the separation between the cross-correlation and auto-correlation traces, and the grating pair induced pulse distortion from the cross-correlation trace, by varying the center frequency of the 0.5-nm optical pulses. This experimental arrangement was detailed in [6] and [7].

III. Results

The wavelengths at which the measurements were performed are labeled on the transmission spectrum. Point A was situated at 1545.00 nm where we expected no grating pair effect. E was at the center of the overlap transmission region. B and F were on opposite sides of the spectrum and had the same transmission as E. D produced the same delay as that of E. C was the spectral midpoint of B and D.

For some of these wavelengths the correlation traces are plotted in Fig. 3(a). The 52-ps separation between the cross-

Manuscript received April 27, 1998. This work was supported by the Air Force Office of Scientific Research (AFOSR) and by the Ballistic Missile Defense Organization (BMDO).

S. Wang, H. Erlig, H. R. Fetterman, and E. Yablonovitch are with the Electrical Engineering Department, University of California, Los Angeles, CA 90095 USA.

V. Grubsky, D. S. Starodubov, and J. Feinberg are with the Physics Department, University of Southern California, Los Angeles, CA 90089-0484 USA.

Publisher Item Identifier S 1051-8207(98)08535-3.

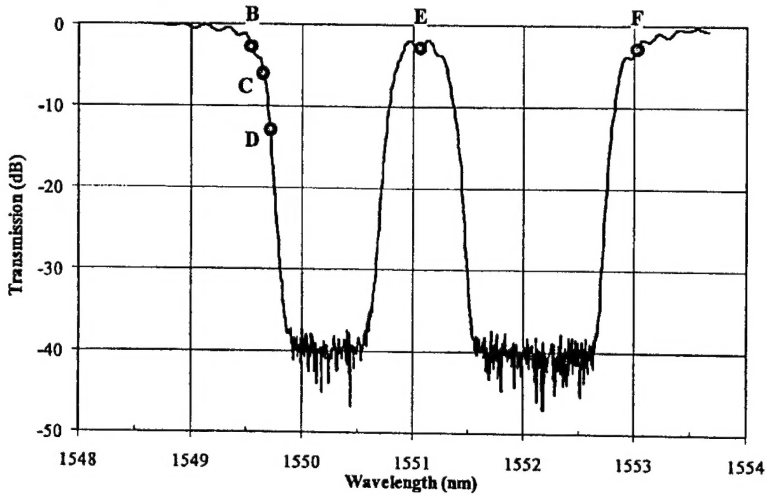

Fig. 1. Transmission spectrum of the grating pair, with bandgap centers at 1550.25 and 1552.10 nm, and 3-dB bandwidths 1.40 and 1.82 nm, respectively. The overlap transmission region had a 1551.05-nm central wavelength, a 0.5-nm 3-dB bandwidth, and −3-dB peak intensity transmission. Operating wavelengths of interest are B: 1549.55 nm, C: 1549.63 nm, D: 1549.70 nm, E: 1551.05 nm, and F: 1553.01 nm.

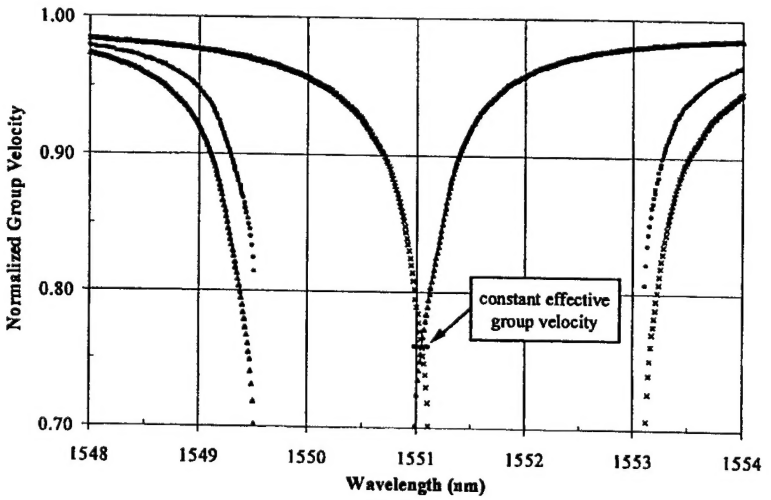

Fig. 2. IFO_Gratings simulation results. (△) normalized group velocity of the grating centered at 1550.25 nm, (×) normalized group velocity of the grating centered at 1552.10 nm, and (•) normalized effective group velocity of the gratings cascaded. The group velocities are normalized to the speed of light in bare fiber. Note the almost flat effective group velocity from 1550.99 to 1551.10 nm.

correlation and auto-correlation traces for point A was intentionally introduced by choosing the grating pair arm ~1 cm longer. Group delays of 11, 13, 15, 15, and 7 ps for points B, C, D, E, and F, respectively, were measured as the additional displacement of the cross-correlation trace relative to the auto-correlation trace. The maximum 15-ps delay corresponds to a group velocity 66% of the speed of light in bare fiber. Assuming a symmetric bandgap for each of the gratings the delay at E was expected to equal that at B plus F, 18 ps. At points E, B, and F the transmission loss amounted to 3 dB. In comparison, point D provided the same delay as E with a 13-dB transmission loss.

A zoom-in view of the cross-correlation traces for several wavelengths is shown in Fig. 3(b). From these we deduced the extent of pulse reshaping. The traces were purposefully superimposed and normalized to their respective peak values for ease of comparison. The structure that appeared at ~90 ps was caused by the leading edge of the auto-correlation trace. The cross-correlation at A exhibited a FWHM of 19.0 ps and it was taken as the reference pulse shape. Operation at E produced a cross-correlation trace with a FWHM of 21.5 ps, 13% larger than that at A. There were three reasons for the slight pulse reshaping at E. First, for a uniform grating, there were oscillations in the transmission and group velocity characteristics [4]. Second, although the GVD was canceled, cubic and higher order dispersion were not [2]. Third, the 0.5-nm pulse bandwidth was larger than the 0.11-nm zero dispersion region. At C and D the cross-correlation FWHM were 28.3 and 29.3 ps, respectively. The pulses widened as expected since at these points there was no dispersion compensation.

IV. Conclusion

We have experimentally demonstrated a grating pair sequence with wavelength dependent group delay exhibiting

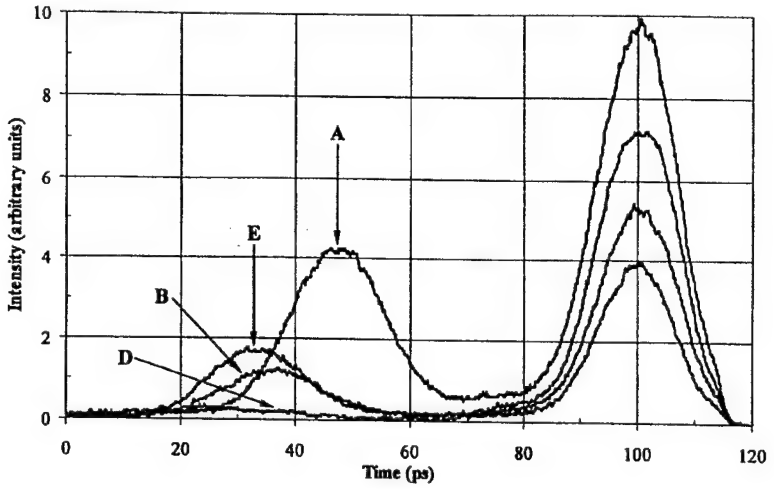

(a)

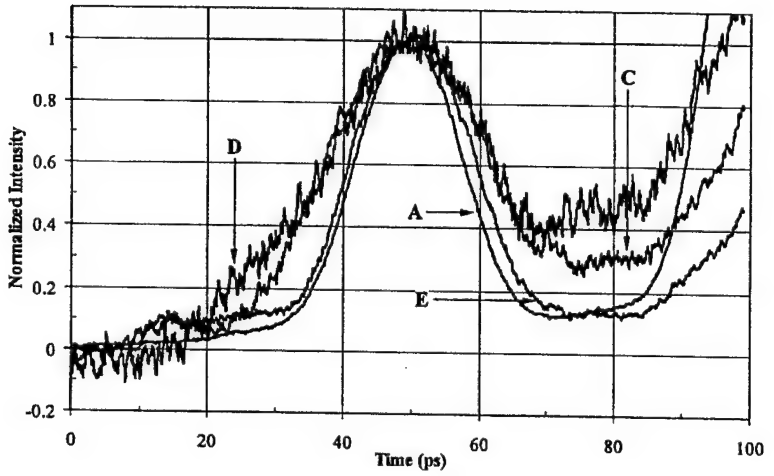

(b)

Fig. 3. (a) Correlation traces for the various operating wavelengths. The auto-correlation traces are located at 100 ps. (b) Zoom-in view of normalized cross-correlation traces for various operating wavelengths defined in Fig. 1.

compensated GVD over a 0.5-nm band. Over this range both gratings contributed to the optical pulse propagation characteristics enabling a 15-ps group delay with 3-dB transmission loss. One possible application of this is in matched filtering schemes, where for a fixed center wavelength one grating in the transmitter stretches the pulse in time while a conjugate grating in the receiver is used for pulse reconstruction. Both gratings can be further expanded as specially designed grating sequences to meet orthogonal code requirements among different channels for CDMA systems.

ACKNOWLEDGMENT

The authors would like to thank Prof. B. Jalali's group for support with the optical instrumentation.

REFERENCES

[1] W. H. Loh, R. I. Laming, N. Robinson, A. Cavaciuiti, F. Vaninetti, C. J. Anderson, M. N. Zervas, and M. J. Cole, "Dispersion compensation over distances in excess of 500 km for 10-Gb/s systems using chirped fiber gratings," *IEEE Photon. Technol. Lett.*, vol. 8, pp. 944–946, July 1996.

[2] N. M. Litchinitser, B. J. Eggleton, and D. B. Patterson, "Fiber Bragg gratings for dispersion compensation in transmission: Theoretical model and design criteria for nearly ideal pulse recompression," *J. Lightwave Technol.*, vol. 15, pp. 1303–1313, Aug. 1997.

[3] N. M. Litchinitser and D. B. Patterson, "Analysis of fiber Bragg gratings for dispersion compensation in reflective and transmissive geometries," *J. Lightwave Technol.*, vol. 15, pp. 1323–1328, Aug. 1997.

[4] B. J. Eggleton, T. Stephens, P. A. Krug, G. Dhosi, Z. Brodzeli, and F. Ouellette, "Dispersion compensation using a fiber grating in transmission," *Electron. Lett.*, vol. 32, pp. 1610–1611, Aug. 1996.

[5] B. J. Eggleton, C. M. de Sterke, and R. E. Slusher, "Nonlinear pulse propagation in Bragg gratings," *J. Opt. Soc. Amer. B*, vol. 14, pp. 2980–2993, Nov. 1997.

[6] S. Wang, H. Erlig, H. R. Fetterman, E. Yablonovitch, V. Grubsky, D. S. Starodubov, and J. Feinberg, "Measurement of the temporal delay of a light pulse through a one-dimensional photonic crystal," *Microwave Opt. Technol. Lett.*

[7] S. Wang, H. Erlig, H. R. Fetterman, V. Grubsky, and J. Feinberg, "One-dimensional photonic crystals for CDMA," in *Multimedia Networks: Security, Displays, Terminals, and Gateways, Proc. SPIE 3228*, 1997, pp. 408–417.

[8] T. M. Goyette, W. Guo, F. C. De Lucia, J. C. Swartz, H. O. Everitt, B. D. Guenther, and E. R. Brown, "Femtosecond demodulation source for high-resolution submillimeter spectroscopy," *Appl. Phys. Lett.*, vol. 67, pp. 3810–3812, Dec. 1995.

Time Stretching of 102-GHz Millimeter Waves Using Novel 1.55-μm Polymer Electrooptic Modulator

D. H. Chang, H. Erlig, M. C. Oh, C. Zhang, W. H. Steier, L. R. Dalton, and H. R. Fetterman

Abstract—**Millimeter (MM)-wave signals at frequencies up to 102 GHz have been time stretched down to 11 GHz using a new wide-band traveling-wave polymer modulator. This is the first application of electrooptic modulators fabricated using the new polymer material PC-CLD, which has demonstrated good optical insertion loss and high nonlinearity at 1.55μm.**

Index Terms—**A/D conversion, electrooptic modulators, PC-CLD, photonic time stretch, polymer modulators.**

I. Introduction

THE ELECTROOPTIC modulator is an enabling component in many photonic and optical/millimeter (MM)-wave systems. As such, its bandwidth often dictates the range of applications which are feasible. Conventional $LiNbO_3$ modulators suffer from a large microwave to optical refractive index mismatch which limits their bandwidth. Polymer modulators have demonstrated promising high-frequency performance, with modulation response from dc out to 110 GHz [1]. Recently, modulators fabricated using the new polymer material PC-CLD have shown significantly reduced optical loss and high nonlinearity at 1.55 μm [2]. As an initial demonstration of its high-frequency capabilities, we have employed time stretch to detect modulation at frequencies up to 102 GHz. Time stretch utilizes linear group velocity dispersion in optic fibers to frequency downshift microwave signals modulated onto optical pulses. The technique has been proposed as a signal preprocessor to extend the upper frequency range of electronic analog/digital (A/D) converters, and has been demonstrated in [3].

Time stretch is related to frequency shifting of modulated optical pulses using time lenses [4], [5]. Time-lens action on electrical signals was also demonstrated earlier in [6]. Unfortunately, the authors of both [3] and [6] use the name "stretch," which can be a source of confusion. The fundamental difference between the two techniques is whether the temporal analog of the imaging condition is obeyed [7]. In [4]–[6], the imaging condition is fulfilled by the use of a quadratic phase (linear frequency) modulation element, which is the analog of a spatial thin lens. In the technique used in [3] and here, temporal magnification relies on dispersion alone. The spatial analog is simply a transparency held before a narrow beam, with the dispersive elements being the space between the beam source, the transparency, and the screen. This greatly simplifies implementation, but incurs a penalty which is analogous to that of an unfocused spatial imaging system. High frequencies are attenuated, imposing a bandwidth limitation which increases in severity with increasing magnification [3].

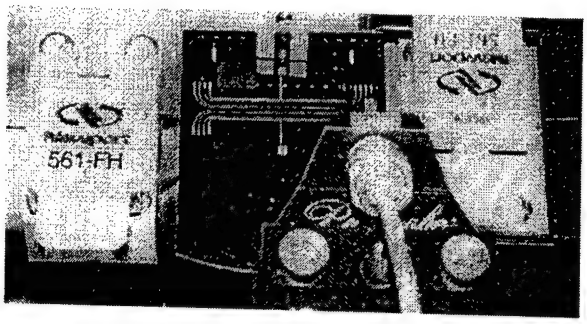

Fig. 1. PC-CLD polymer modulator in experimental setup with fiber coupling and V-band microwave probe. Light is coupled into and out of the modulator using fibers tipped with cylindrical lenses, which minimizes the coupling loss to about 1.5 dB/facet.

II. The PC-CLD Modulator

Fig. 1 shows the experimental unpackaged PC-CLD modulator used here. The substrate is gold-plated silicon, onto which the active material is spun and corona poled. Ridge optical waveguides are fabricated into the active material to form Mach–Zehnder interferometers (MZI's). The substrate serves as the ground plane for the microstrip lines patterned above the optical waveguides. Details on the fabrication and characterization of the device are discussed in [2]. The modulating electrical signal is injected from a coplanar probe near the input fiber. The probe shown is rated to 67 GHz; for modulation at 102 GHz, one with a W-waveguide input is substituted.

Figures of merit for the PC-CLD modulator are preliminary, as key elements such as interaction length and microstrip design are being optimized. Measurements conducted on this particular sample shows $V_\pi \approx 5$ V and total insertion loss of 12 dB. The device shows a flat frequency response to 40 GHz. Although operation well above 40 GHz has been demonstrated (for example in this experiment), a detailed frequency response measurement remains to be performed. While the device has survived repeated operation at 5–10 mW of optical power, long-term power limitations will be established once packaged units with fiber-pigtails are fabricated.

Manuscript received November 29, 1999; revised February 9, 2000. This work was supported under grants from the AFOSR and DARPA.

D. H. Chang and H. R. Fetterman are with the Department of Electrical Engineering, University of California at Los Angeles, Los Angeles, CA 90095 USA (e-mail: dhchang89@alum.mit.edu).

H. Erlig is with Pacific Wave Industries, Los Angeles, CA 90024 USA.

M. C. Oh, C. Zhang, W. H. Steier, and L. R. Dalton are with the Department of Electrical Engineering and Chemistry, University of Southern California, Los Angeles, CA 90098 USA.

Publisher Item Identifier S 1041-1135(00)03685-2.

III. Time-Stretch Theory

Time stretch exploits group velocity dispersion (GVD) to temporally expand a pulse while preserving its envelope shape. Details of the theory are in [3]. Two long fiber spools of length L_1 and L_2 are used, with the modulator in between. The relevant stretch factor M is the width of the pulse exiting L_2 compared to that exiting L_1. If we denote by τ_0 the pulse width exiting the laser and $\delta\tau_1$, $\delta\tau_2$ the additional broadening from L_1, L_2, respectively, then

$$M = \frac{\tau_0 + \delta\tau_1 + \delta\tau_2}{\tau_0 + \delta\tau_1} = 1 + \frac{\delta\tau_2}{\tau_0 + \delta\tau_1} \approx 1 + \frac{L_2}{L_1} \quad (1)$$

if $\tau_0 \ll \delta\tau_1$. This is certainly true in our system, where τ_0 (autocorrelation) $\approx$ 150 fs, while $\tau_0 + \delta\tau_1 > 1$ ns.

IV. Experimental Results

The optical source is a passively mode-locked Er^{3+}-doped fiber laser with a 50-nm pulse bandwidth at 1.55 μm and a 40-MHz repetition rate. To ensure linear propagation, the optical power is attenuated with a combination of neutral-density plates and variable attenuator. The output of the attenuator is propagated through L_1 (standard SMF) and a fiber-polarization controller before entering the modulator. The modulated output is amplified in an Er^{3+}-doped fiber amplifier before entering the L_2 spools, also SMF. The output of the L_2 spools is detected by a 45-GHz bandwidth photodiode and amplified by a 32-dB microwave amplifier. The specified passband of the amplifier is 8–12 GHz.

Four modulation sources are used: a sweep oscillator (to 40.8 GHz), a synthesizer (to 50 GHz), a GUNN oscillator (61.2 GHz), and a Klystron (102 GHz). Data are captured with both a spectrum analyzer and a sampling oscilloscope. To see the effect of time stretching directly in the time domain would require locking the laser pulse rate to the modulating source, an unavailable option for the last three sources. We instead rely on an indirect signature in the frequency domain, since the basic operation of time stretching has already been demonstrated [3]. The combined effect of modulation and subsequent time stretching is a frequency shifting of the carrier pulses' power spectral density to the stretched modulation frequency, which is observable using the spectrum analyzer.

Fig. 2 shows the unmodulated pulse after traversing the entire system, with $L_1 = 1.5$ and $L_2 = 4.5$ km. As can be seen, the pulse is much wider than its initial 150-fs width, and has acquired ripples which translate to "twin lobes" in the power spectral density. A fast Fourier transform (FFT) performed on the time-domain pulse corroborates the spectrum analyzer data. The source of the ripples has been isolated to the slight effective length mismatch between the two arms of the MZI. While such a mismatch is routinely compensated for with a bias voltage when modulating a CW beam, it produces intensity ripples in a highly chirped pulse. The ripple period is a function of the chirp parameter and the effective temporal mismatch. In addition, since waves of different polarizations in the optical waveguide suffer different mismatches, the overall output pulse shape is highly sensitive to the input polarization.

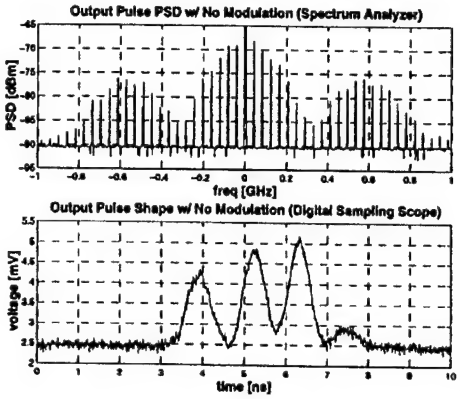

Fig. 2. Pulse power spectral density (PSD) and temporal shape with no modulation. The spike at dc is due to the noise floor.

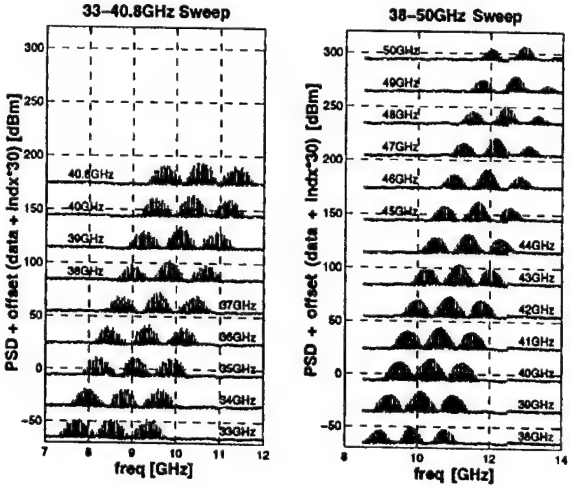

Fig. 3. Spectrum analyzer data for two modulation frequency sweeps. The spectra are replicas of that in Fig. 2 shifted to the stretched modulation frequency.

In an A/D application, the pulse ripples compete with the modulated signal and would be an undesirable feature which must be eliminated in postprocessing at the expense of conversion accuracy. For this experiment, no such compensation is required to recognize the effect of modulation, which simply frequency shifts the entire PSD waveform. The spacing between the PSD spectral lines is equal to the 40-MHz laser repetition rate, as expected.

Fig. 3 shows the shifted spectra as the modulation frequency is swept from 33 to 50 GHz, with $L_1 = 1.5$ and $L_2 = 4.5$ km. The centers of the captured spectra are extracted and plotted against the modulation frequency in Fig. 4. As expected, the relationship is linear; the fitted M is 3.86. The "upper lobes" of the spectra near 50 GHz are distorted by the bandwidth of the 8–12-GHz microwave amplifier.

In Fig. 5, a GUNN oscillator with a measured peak at 61.8 GHz is used to drive the modulator. To bring the stretched waveform back into the microwave amplifier's passband, L_2 is increased to 6.5 km, while L_1 remains at 1.5 km. In all other aspects, the system remains unchanged from the 33- to 50-GHz data set. The measured M is 5.13.

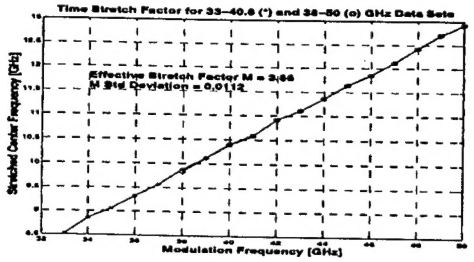

Fig. 4. Effective stretch ratio calculated for data sets seen in Fig. 3. From the data, $M_{\text{eff}} = 3.86$, with a 1σ deviation from linearity of 1.1%. The calculated value from (1) is $M = 4$.

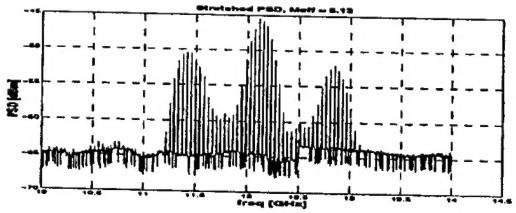

Fig. 5. GUNN-oscillator source with output measured at 61.81 GHz is time stretched to 12.05 GHz ($M = 5.13$). The pulse shape remains similar to that in Fig. 3.

Finally, time stretch using a Klystron oscillator at 101.7 GHz (as measured by a frequency counter and harmonic mixer) is shown in Fig. 6. Now $L_1 = 0.5$ and $L_2 = 5.0$ km to bring M to 11; the measured ratio is 9.8. The large change in fiber arrangement alters the pulse shape, as can be inferred by the zero-modulation PSD in Fig. 6. With the signal level available, only the top portion rises above the noise floor in the stretched data.

The discrepancies between measured and calculated stretch ratios stem from dispersion introduced ahead of the modulator by the variable attenuator and a 50-m fiber patch cord connecting the laser to the L_1 spool. The effective M from (1) is

$$M_{\text{eff}} = 1 + \frac{L_2}{L_1 + \delta}$$

where δ represents dispersion equivalent to that length of SMF. Solving for δ in the three frequency regimes using measured M_{eff}'s of 3.86, 5.13, and 9.80 gives self-consistent values of 73, 74, and 68 m, respectively.

V. Conclusion

This experiment is the first reported application of electrooptic modulators fabricated from the new polymer material PC-CLD. We have utilized time stretching to show modulation at up to 102 GHz. It extends the previously demonstrated high-frequency capabilities of polymer modulators to important 1.55-μm applications.

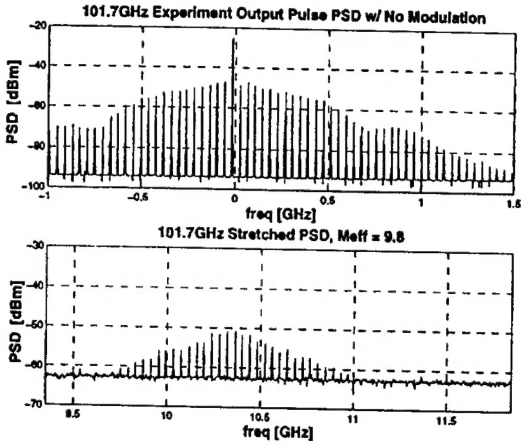

Fig. 6. Stretch experiment with 101.7-GHz Klystron source. Top trace is zero-modulation spectrum, differing slightly from Fig. 2 because increasing M from 4 to 11 has changed the pulse shape. Bottom trace shows stretched spectrum with $M_{\text{eff}} = 9.8$. The frequency axes for both plots have the same scaling and span.

It must be noted that time stretching suffers an inherent bandwidth limitation, analogous to defocused imaging in the spatial domain. As calculated in [3], the intensity transmission versus modulation frequency consists of a series of deep notches; a larger M results in a lower first-notch frequency. For this experiment, the narrow-band modulation signals were chosen to avoid the notch frequencies, an unavailable option for a wide-band signal. In an A/D preprocessor application, the actual system bandwidth is limited both by the modulator and the maximum stretch ratio required to map into the A/D converter's operating range.

Acknowledgment

The authors would like to thank I. Poberezhskiy, Drs. B. Tsap and Y. Chang, H. Zhang, Drs. F. Coppinger and B. Jalali, and A. S. Bhushan for their assistance.

References

[1] D. Chen, H. R. Fetterman, A. Chen, W. H. Steier, L. R. Dalton, W. Wang, and Y. Shi, "Demonstration of 110 GHz electro-optic polymer modulators," *Appl. Phys. Lett.*, vol. 70, no. 25, pp. 3335–3337, 1997.

[2] M. C. Oh, H. Zhang, A. Szep, V. Chuyanov, W. H. Steier, C. Zhang, and L. R. Dalton, "Practical electro-optic polymer modulators using PC/CLD," in *Organic Thin Films for Photonic Applications*, Sept 1999.

[3] F. Coppinger, A. S. Bhushan, and B. Jalali, "Photonic time stretch and its application to analog-to-digital conversion," *IEEE Trans. Microwave Theory Tech.*, vol. 47, no. 7, pp. 1309–1314, 1999.

[4] C. V. Bennet and B. H. Kolner, "Upconversion time microscope demonstrating 103X magnification of femtosecond waveforms," *Opt. Lett.*, vol. 24, no. 11, pp. 783–785, June 1999.

[5] C. V. Bennett, R. P. Scott, and B. H. Kolner, "Temporal magnification and reversal of 100 Gb/s optical data with an up-conversion time microscope," *Appl. Phys. Lett.*, vol. 65, no. 20, pp. 2513–2515, Nov. 1994.

[6] W. J. Caputi, "Stretch: A time-transformation technique," *IEEE Trans. Aerosp. Electron. Syst.*, vol. AES-7, pp. 269–278, March 1971.

[7] B. H. Kolner, "Space–time duality and the theory of temporal imaging," *IEEE J. Quantum Electron.*, vol. 30, pp. 1951–1963, Aug. 1994.

Phased-Array Optically Controlled Receiver Using a Serial Feed

Boris Tsap, Yian Chang, Harold R. Fetterman, *Fellow, IEEE*, A. F. J. Levi, David A. Cohen, and Irwin Newberg, *Member, IEEE*

***Abstract*—Extension of a new optically controlled serially fed phased-array system to the receive mode of operation has been demonstrated. Our system uses the pulsed nature of microwave radars in a manner similar to clocked systems used in digital configurations. This novel approach requires only the use of one tunable laser, one optical modulator, and one chirped fiber grating unit. In this letter, we present an experimental demonstration of a two-element serially fed wide frequency range receiver that validates the feasibility of this novel concept. Our system can be readily expanded with multiple elements and transmit/receive modules for a complete phased array system.**

***Index Terms*—Directional communications, fiber gratings, optical control, optical fiber delay line, phased-array radar.**

I. Introduction

WE HAVE recently reported the development of a novel optically controlled phase array transmit configuration, suitable for numerous applications, including phased array radar and directional data communications [1]–[3]. The serial-feed concept used in these systems represented a departure from conventional parallel-feed approaches, which are very laser intensive [4]–[14]. Our system's use of a single wavelength tunable laser, one modulator, and one fiber grating time delay element provided a major simplification in the number of required optical components. In this letter, we report the demonstration of the receive portion of this concept using a two-element receiver with observation directions ranging from $+30°$ to $-30°$. The dependence on one time delay unit to provide time/phase shifts for all of the antenna elements distinguishes this serially-fed system from previously implemented receive systems [13], [15]. Our introduction of a chirped fiber grating to the system enhances its capability by making its directional operation continuously variable. Combined with our transmit capability [1], and with the use of a T/R switch, this new design can now be extended to a complete transmit/receive radar system.

Manuscript received June 30, 1997; revised October 17, 1997. This work was supported in part by the AFOSR under Dr. Howard Schlossberg, in part by the NCIPT, and in part by the DOD SBIR under Contract DAAH01-97-C-R026.

B. Tsap is with Pacific Wave Industries, Inc., Los Angeles, CA 90024 USA.

Y. Chang and H. R. Fetterman are with the Department of Electrical Engineering, University of California at Los Angeles, Los Angeles, CA 90095 USA.

A. F. J. Levi and D. A. Cohen are with the Department of Electrical Engineering, University of Southern California, Los Angeles, CA 90089-1111 USA.

I. Newberg is with the Radar and Communication Systems, Hughes Aircraft Company, Los Angeles, CA 90009-2426 USA.

Publisher Item Identifier S 1041-1135(98)01269-5.

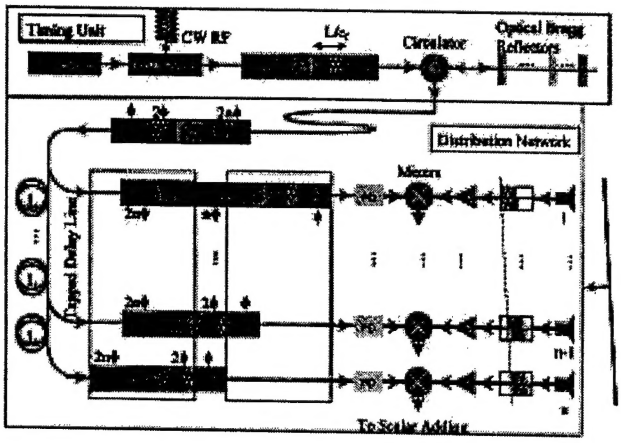

Fig. 1. Basic serially fed receive mode configuration for an array of n elements. A chirped fiber grating in conjunction with a tunable laser provides the necessary phased delays for virtually continuous directional operation. A second tapped delay line in parallel can be added to achieve almost continuous temporal operation.

II. Serially Fed Receiver Configuration

The serially fed receiver consists of a timing unit and a serial to parallel conversion distribution network as shown in Fig. 1. The timing unit sequentially generates delays designated for a given direction of observation. The distribution network then transforms these delays into parallel signals and feeds them to the antenna elements.

In the basic receive configuration (Fig. 1), the train of (L/c_f)-long laser light pulses, where L is the tapped fiber delay length and c_f is speed of light in fiber, is modulated at the desired microwave frequency, and directed through an optical circulator to a fiber grating. By reflecting from a particular point on the fiber grating a wavelength-selected phase shift is imposed onto each modulated optical pulse. The returned light from the third port of the circulator enters the distribution network which supplies each mixer with the local oscillator (LO) signal for mixing with the received microwave signal. Assume that the tapped delay line is loaded sequentially with $2n$ pulses from a tunable laser each carrying the LO signals that are phase shifted by $\phi, 2\phi, \cdots, 2n\phi$, respectively, to the mixers. The tunable laser must switch wavelengths on the order of a ns and therefore has little effect on typical radar signals which have durations of hundreds, and even thousands, of nanoseconds. At the beginning of the receive mode of operation, the first pulse supplies the last mixer and the nth pulse supplies the first mixer. After an interval L/c_f in

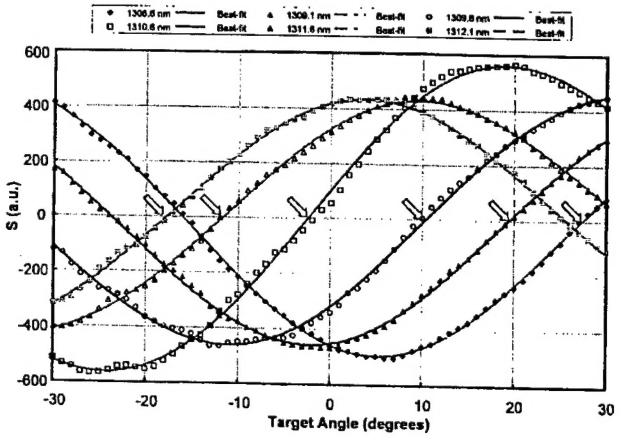

Fig. 2. Target scanning with the receiver pointed to six different "listening" directions, defined by the tunable laser wavelength λ_t. In this demonstration, experimentally determined "listening" directions correspond to the angles where $S = 0$ and $S' > 0$.

time, the second pulse will reach the nth mixer and become its LO signal carrier. At the same time, the $(n+1)$th pulse will be supplying the first mixer and the cycle continued. Note that the receiver continues to "listen" in the same direction after each wavelength progression because only the relative phases between mixers (differential phase ϕ) are important. This wavelength progression repeats until the last loaded pulse reaches the first mixer.

At this point, there would be a loss of duty cycle for the simplest configuration while the line is reloaded. However, in order to achieve almost continuous operation, our design can incorporate the option of a second tapped delay line with an extra nL delay length which can be switched to feed each mixer the appropriate phase. Although, as in our initial transmit experiment a two-laser switch system was used, we have utilized a linearly chirped grating, which along with a tunable DBR laser will provide almost continuous scanning for the ultimate system.

III. Experiment

In an experimental demonstration with a two-element array, we used two external cavity wavelength tunable lasers in conjunction with two optical modulators to simulate a single fast tunable laser. The wavelength of the first laser was fixed at λ_f and the wavelength λ_t of the second laser was tuned to different values to control the "listening" direction of the receiver. A continuously chirped fiber grating centered at 1310 nm with a 10-nm bandwidth (>97% reflectivity) was used as the wavelength sensitive element. Phase delayed signals corresponding to the reflections of λ_f and λ_t were generated by the basic true time delay (TTD) timing unit used in the transmit configuration and, therefore, yielded squint-free operation. An RF signal was simultaneously fed to a transmitting horn placed on a rotating stage to simulate the signal returned from a target. The RF signal picked up by each of the receiving antenna elements was fed to the RF port of a mixer. The LO input of the mixer at each element was provided with the phase delayed signal from the timing unit and photodiode. Because the target distance was considered unknown, quadrature mixers were used to provide homodyne IF signals in two quadrants. The two outputs of the mixer associated with the first antenna element contain dc components given by

$$V_{\sin}^{\mathrm{I}} = A_{\mathrm{I}} B_{\mathrm{I}} \sin(\phi - \Phi_1) \quad V_{\cos}^{\mathrm{I}} = A_{\mathrm{I}} B_{\mathrm{I}} \cos(\phi - \Phi_1).$$

For the outputs of the mixer associated with the second antenna element, we have

$$V_{\sin}^{\mathrm{II}} = A_{\mathrm{II}} B_{\mathrm{II}} \sin(\Delta - \Phi_1) \quad V_{\cos}^{\mathrm{II}} = A_{\mathrm{II}} B_{\mathrm{II}} \cos(\Delta - \Phi_1)$$

where A_{I} and A_{II} are proportional to the LO amplitudes sent to the mixers, B_{I} and B_{II} are proportional to the received RF amplitudes, Φ_1 is an unknown phase in the received RF signals due to the unknown target distance, ϕ is the phase difference between the LO signals (from the timing unit), $\Delta = (d\omega \sin\theta)/c$ is the phase difference between the received RF signals due to the different path lengths from the target, θ is the target angle, and d is the spacing between the antenna elements. The four outputs of the mixers were fed to a computer for processing. The computer calculated the final result in the form

$$S = V_{\cos}^{\mathrm{I}} \cdot V_{\sin}^{\mathrm{II}} - V_{\sin}^{\mathrm{I}} \cdot V_{\cos}^{\mathrm{II}} = A_{\mathrm{I}} A_{\mathrm{II}} B_{\mathrm{I}} B_{\mathrm{II}} (\Delta - \phi). \quad (1)$$

The phase difference between the LO signals is set in the timing unit by the fiber grating for each wavelength pair $\lambda_f - \lambda_t$ and is described by

$$\phi = k(\lambda_t - \lambda_f)\omega$$

where k is a parameter involving the chirp of the fiber grating. For a given target direction, θ can be extracted by plotting $S[\phi(\lambda_t)]$ for different λ_t. The calculated function S in (1) is zeroed, with a positive slope, when $(d\sin\theta)/c = k(\lambda_t - \lambda_f)$. Therefore, the target angle can be written as

$$\theta = \sin^{-1}[ck(\lambda_t - \lambda_f)/d]. \quad (2)$$

In this feasibility demonstration, the receiver had only two elements and to increase the resolution of the system, we had chosen to use the function S in (1) to determine the target angle because of its sensitivity near $(d\sin\theta)/c = k(\lambda_t - \lambda_f)$.

To demonstrate the ability of the system as a phased array radar receiver, we chose six different wavelength pairs to deliver the LO signals; effectively, the receiver was used to "listen" to six different directions. For a selected direction (wavelength pair), the target angle was changed from −30° to 30° with a step size of 1°. As shown above at the right "listening" direction the S function is zero with a positive slope. In these experiments, the RF frequency was set to 8 GHz, λ_f was kept at 1310.6 nm and λ_t was tuned to six different wavelengths. Fig. 2 shows the corresponding S function versus the target angle for each wavelength pair. The least square best-fit functions were calculated and used to determine the target directions with higher accuracy. The measured target angles (corresponding to the angles where $S = 0$ and $S' > 0$ in Fig. 2) are −17.7°, −11.6°, −2.4°, 10.4°, 19.4°, and 27.4°. The theoretically calculated six "listening" directions, using (2), are −19.3°, −12.8°, 0°, 12.8°, 19.3°, and 26.2°. The measured values are well within the expected 3° of the two antenna element theoretical values.

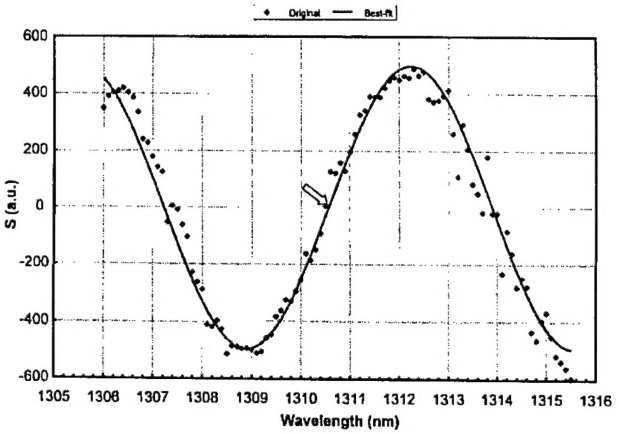

Fig. 3. Wavelength scanning with the target located at 0° and the fixed wavelength $\lambda_f = 1310.55$ nm. Using a best-fit function to the sine function, the experimentally determined target direction is $\theta = 0.6°$.

In another experimental modality to demonstrate the capability of changing the "listening" direction continuously, the target angle was fixed at 0° and λ_f was set to 1310.6 nm. The wavelength λ_t was then scanned from 1306.0 to 1315.5 nm with a step size of 0.1 nm determined by the resolution of the tunable laser. The S function versus the wavelength λ_t is shown in Fig. 3. The solid line is the best-fit sine-function that has a zero value (with a positive slope) at the wavelength $\lambda_t = 1310.60$ nm corresponding to 0.6° according to (2). The results show excellent agreement with predictions and indicate that the serial system works well in the receive mode.

IV. Conclusion

We have successfully demonstrated a receive mode operation of a serially fed optically controlled phased array system. It uses the same basic elements as the previously reported transmitter and completes the serial system.

For a practical system with multiple elements, the mixer outputs would be processed in the following way:

$$M = \left(\sum_i V_{\cos}^{(i)}\right)^2 + \left(\sum_i V_{\sin}^{(i)}\right)^2. \tag{3}$$

When the signal arrives in from the desired direction, the angular phase dependency is removed by mixing with the selected LO signals for that direction; the scalar function M is maximized by this process. In a radar application, this scalar signal M can then be used to determine the target distance. In a practical multiple-element radar system, the beam width will be much narrower than that of our two-element array. Therefore, the M function in (3) can be used to sum the mixer outputs together for further processing. M will be maximized as a sharp peak only at the selected direction because the mixer outputs are "in phase" at this receive angle and "out of phase" elsewhere.

In a pulsed transmit/receive radar system, once a RF pulse has been transmitted, the system has to switch to the receive mode to listen for the echo. The conjugate differential phase (ϕ) of that used in transmit ($-\phi$) is now used in the receive mode since the mixers generate a difference frequency and subtract the phases of the two input signals to be used in forming the scalar quantity M. This phase requirement can be achieved by using the fiber grating in the reverse direction or by using the transmit wavelengths in reverse order. This technique provides the wide frequency range squint-free receiver steering since real-time delays, generated in the fiber grating, are used to obtain the phase angles.

The extension of the two-element serially fed optically controlled system to the receive mode has been presented. Of greater importance, however, is that it is now possible to implement the concept of a serial feed in a complete radar system, which will require a transmit/receive switch module and a dual feed line for a continuous operation. Finally, because of its simplicity and the significant reduction in the number of optical components, this system has major advantages over proposed conventional parallel configurations and is one of the few which have actually been demonstrated [13], [15].

References

[1] Y. Chang, B. Tsap, H. R. Fetterman, D. A. Cohen, A. F. J. Levi, and I. Newberg, "Optically controlled serially fed phased-array transmitter," *IEEE Microwave Guided Wave Lett.*, vol. 7, pp. 69–71, Mar. 1997.

[2] D. A. Cohen, Y. Chang, A. F. J. Levi, H. R. Fetterman, and I. Newberg, "Optically controlled serially fed phased array sensor," *IEEE Photon. Technol. Lett.*, vol. 8, pp. 1683–1685, Dec. 1996.

[3] D. A. Cohen, A. F. J. Levi, Y. Chang, H. R. Fetterman *et al.*, "Video broadcast using an optically controlled serially-fed phased-array antenna," in *Proc. SPIE*, 1996, vol. 2844, pp. 258–268.

[4] D. Dolfi, P. Joffre, J. Antoine, J.-P. Huignard, D. Philippet, and P. Granger, "Experimental demonstration of a phased-array antenna optically controlled with phase and time delays," *Appl. Opt.*, vol. 35, no. 26, pp. 5293–5300, 1996.

[5] D. Dolfi, P. Joffre, J. Antoine, J.-P. Huignard, D. Philippet, P. Granger, and J. Chazelas, "Photonics for phased array radars," in *Proc. SPIE*, 1995, vol. 2560, pp. 158–165.

[6] H. R. Fetterman, Y. Chang, D. C. Scott, S. R. Forrest, F. M. Espiau, M. We, D. V. Plant, J. R. Kelly, A. Mather, W. H. Steier, R. M. Osgood, "Optically controlled phased array radar receiver using SLM switched real time delays," *IEEE Microwave Guided Wave Lett.*, vol. 5, pp. 414–416, Nov. 1995.

[7] L. Xu, R. Taylor and S. R. Forrest, "True time-delay phased-array antenna feed system based on optical heterodyne techniques," *IEEE Photon. Technol. Lett.*, vol. 8, pp. 160–162, Jan. 1996.

[8] R. D. Esman, M. Y. Frankel, J. L. Dexter, L. Goldberg, M. Parent, D. Stilwell, and D. Cooper, "Fiber-optic prism true time-delay antenna feed," *IEEE Photon. Technol. Lett.*, vol. 5, pp. 1347–1349, Nov. 1993.

[9] A. Molony, C. Edge, and I. Bennion, "Fiber grating time delay element for phased array antennas," *Electron. Lett.*, vol. 31, no. 17, pp. 1485–1486, 1995.

[10] N. A. Riza and N. Madamopoulos, "Phased-array antenna, maximum-compression, reversible photonic beam former with ternary designs and multiple wavelength," *Appl. Opt.*, vol. 36, no. 5, pp. 983–996, 1997.

[11] D. T. K. Tong and M. C. Wu, "Programmable dispersion matrix using Bragg fiber grating for optically controlled phased array antennas," *Electron. Lett.*, vol. 32, no. 17, pp. 1532–1533, 1996.

[12] W. D. Jemison, T. Yost, and P. R. Herczfeld, "Acoustooptically controlled true time delays: Experimental results," *IEEE Microwave Guided Wave Lett.*, vol. 6, pp. 283–2855, Aug. 1996.

[13] J. J. Lee, R. Y. Loo, S. Livingstone, V. I. Jones, J. B. Lewis, H.-W. Yen, G. L. Tangonan, and M. Wechsberg, "Photonic wideband array antennas," *IEEE Trans. Antennas Propagat.*, vol. 43, pp. 966–982, Sept. 1995.

[14] A. P. Goutzoulis, J. M. Zomp, B. K. Davies, and P. Hrycak, "Hardware compressive, true time-steering for control of phased array antennas," Rome Lab. Rep., no. RL-TR-95-293, Jan. 1996.

[15] M. Y. Frankel and R. D. Esman, "True time-delay fiber-optic control of an ultrawideband array transmitter/receiver with multibeam capability," *IEEE Trans. Microwave Theory Tech.*, vol. 43, pp. 2387–2394, Sept. 1995.